SECURITY CLASSIFICATION OF THIS PAGE (When

REPORT DOCUMENTAT

AD-A244 841

STRUCTIONS
MPLETING FORM
ALOG NUMBER

1. REPORT NUMBER

ARO 25177.15-MS

4. TITLE (and Subtitle)

PROCESSING, STRUCTURE AND PROPERTIES OF HEAVILY DEFORMED IN SITU COMPOSITES

5. TYPE OF REPORT & PERIOD COVERED

Final: 6/1/88-5/31/91

6. PERFORMING ORG. REPORT NUMBER

7. AUTHOR(s)

T. H. Courtney

8. CONTRACT OR GRANT NUMBER(s)

DAAL03-88-K-0091

9. PERFORMING ORGANIZATION NAME AND ADDRESS

T. H. Courtney, Department of Mat. Sc.
Thornton Hall, University of Virginia
Charlottseville, Va. 22903-2442

10. PROGRAM ELEMENT, PROJECT, TASK AREA & WORK UNIT NUMBERS

11. CONTROLLING OFFICE NAME AND ADDRESS

U. S. Army Research Office
Post Office Box 12211
Research Triangle Park, NC 27709

12. REPORT DATE

July 5, 1991

13. NUMBER OF PAGES

29

14. MONITORING AGENCY NAME & ADDRESS(if different from Controlling Office)

15. SECURITY CLASS. (of this report)

15a. DECLASSIFICATION/DOWNGRADING SCHEDULE

16. DISTRIBUTION STATEMENT (of this Report)

Approved for public release; distribution unlimited.

DTIC
ELECTE
JAN 10 1992
S D

17. DISTRIBUTION STATEMENT (of the abstract entered in Block 20, if different from Report)

18. SUPPLEMENTARY NOTES

THE VIEW, OPINIONS, AND/OR FINDINGS CONTAINED IN THIS REPORT ARE THOSE OF THE AUTHOR(S) AND SHOULD NOT BE CONSTRUED AS AN OFFICIAL DEPARTMENT OF THE ARMY POSITION, POLICY, OR DECISION, UNLESS SO DESIGNATED BY OTHER DOCUMENTATION.

19. KEY WORDS (Continue on reverse side if necessary and identify by block number)

Composite Materials, Mechanical Alloying, Hot Isostatic Pressing
Amorphous Materials, Microstructural Stability

20. ABSTRACT (Continue on reverse side if necessary and identify by block number)

This report describes research accomplishments in several areas relative to the general theme of the program. Microstructural stability, particularly stability in heavily deformed in situ composites, has been studied and classified systematically. Mechanisms and avenues for the breakdown of plate like structures have been identified, and the conditions under which the several

DD FORM 1473 EDITION OF 1 NOV 65 IS OBSOLETE

92-00678

92 1 7 054

SECURITY CLASSIFICATION OF THIS PAGE (When Data Entered)

92 1 8 068

BLOCK 20

types of instability take place have been specified. Clarification of the strengthening mechanisms that operate in deformation processed composite materials has been made. Tensile and fracture characteristics of metal-metallic glass laminates have been investigated. Laminate fracture toughnesses are much greater than for the metallic glass. This is due to a crack closing force provided by the metal for which the crack lags behind that in the glass. The toughening mechanism has been described in quantitative as well as qualitative terms. Fundamental modeling of the mechanical alloying process has been made from both a mechanics standpoint and a kinetic one. Experimental studies complement analysis. Amorphization behavior of Ni-W alloys during mechanical alloying has been systematically investigated, as has the subsequent crystallization behavior of these materials. Consolidation of mechanically alloyed Ni-W and Cu-Nb materials has been investigated. Models of hot isostatic pressing have been used to mimic the densification behavior of mechanically alloyed materials for this process.

FINAL REPORT: PROCESSING, STRUCTURE AND PROPERTIES OF HEAVILY DEFORMED TWO PHASE MATERIALS

Period: June 1, 1988 - May 31, 1991

I. INTRODUCTION AND OVERVIEW

This report summarizes work accomplished during the above period and that that is still in progress in this program. By the standards of publications and student support, the program has been productive. As noted in Appendix B, two M.S. degrees and one Ph.D. have been awarded during the period covered by this report. In addition, one M.S. degree will be completed shortly and an additional Ph.D. student will complete her work soon (probably within six months). Appendix A lists the publications which resulted from this grant. Nineteen publications are listed in this appendix, including three that are in press or in review. Four of the publications listed resulted from a previous ARO grant (1985-88); they are presented in Appendix A since they were not in print at the time of the final report submitted in 1988. It is noteworthy that five of the publications listed were made in response to invitations, including a review article for the Treatise of Materials Science and Technology and an invited paper for the 12th Riso International Conference on Metallurgy and Materials Science: Metal Matrix Composites.

The publications of Appendix A are divided into four broad areas in which we were engaged these past three years: 1) Microstructural Evolution and Stability, 2) Metal-Metallic Glass Composites, 3) Deformation Processed Composite Materials (DPCM) and 4) Mechanical Alloying (MA) Processing. These form the basis for the division of the report following. We do not provide details of all of the individual papers. Instead, we attempt here to present a synthesis of them. More details are provided for the work that is relatively new, and which has not yet been published. These are also the areas being pursued under a new grant from the Army Research Office.

2. RESEARCH PROGRESS

A. Microstructural Evolution and Stability

Most of the research in this area resulted from the previous ARO grant (A1-A3)*. In brief, we were concerned with the thermal stability of lamellar or plate like microstructures. This is an intriguing problem as lamellar structures are inherently shape stable. That is they possess no finite radii of curvature, and thus are considered immune to the types of coarsening processes to which fibers and spheres are subject. Coarsening of lamellar structures is instigated by microstructural "defects", either in

*- The reference notation applies to the papers listed in Appendix A.

the form of lamellar terminations or internal boundaries within the lamellae. We experimentally identified (A1) three types of lamellar instabilities, as indicated schematically in Fig. 1. We called these cylinderization (the plate evolves into a cylinder), edge spheroidization (rows of spheres are formed along the plate edge) or boundary splitting (the plates are severed as a result of mass transport occurring in the vicinity of the junction between the internal boundary and the interphase boundary).

We modeled the structural breakdown of "isolated" plates (A2) (i.e., plates for which interplate mass transfer can be neglected). The results were presented in the form of plate instability diagrams, examples of which are given in Figs. 2. The diagrams have axes of plate aspect ratio (the ratio of the length between terminations to the plate thickness) and the ratio of the internal boundary energy to the interphase boundary energy. Regions within the diagrams identify the dominant instability mechanism. The respective areas corresponding to the dominant mechanisms vary, depending upon whether surface or volume diffusion dominates the instability process (Fig. 2a vs. Fig. 2b). In both cases, though, cylinderization is favored by plates with low aspect ratios, edge spheroidization for plates with high aspect ratios and relatively low values of the internal boundary energy, and boundary splitting is dominant for plates with high aspect ratios and relatively high values of the internal boundary energy. Contours of the time required to effect the instability can be superimposed on the diagrams, as is done in Figs. 2. The instability times are expressed in terms of a base time which depends on various thermodynamic (e.g., interphase surface energy) and kinetic (e.g. diffusion coefficient) factors as well as the plate thickness.

The exercise described above was an approximate one. That is, instability times were calculated using "educated guesses" with regard to the average diffusion distance and area. As a consequence, we then "checked" the adequacy of these approximations (for boundary splitting and cylinderzation) via a finite difference approach (A3). For the most part, the finite difference results were in good accord with our approximations. However, the finite difference technique underscored some subtleties that can occur in plates having low aspect ratios. In particular, a "plate like" structure can sometimes be stabilized in these circumstances as a result of the "competition" between boundary splitting and cylinderization which have antiparallel mass transfer directions.

As mentioned, (A1-A3) were based on work conducted during the period of our previously sponsored program. However, as a result of them we were invited to prepare two other papers summarizing and extending our ideas. One such paper (A4) is, more or less, a synthesis of (A1-A3) which places the problem in a broad context. We might add that a review of this paper (by Jacques E. Schoutens, Journal of Materials, February, 1991) remarked "It is pleasant and even entertaining to read about such an esoteric

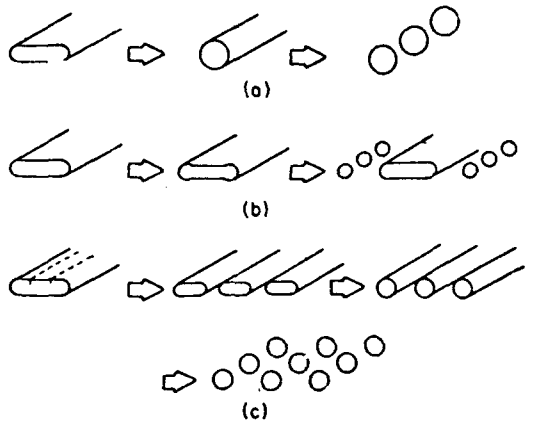

Fig. 1: Schematic of instabilities that can take place in plate like structures. (a) Cylinderization is instigated by plate terminations, having a finite radius of curvature. The process is caused by mass transfer from plate terminations to the plate broad faces. (b) Edge spheroidization is also initiated by terminations. Mass is transferred along the long axis of the plate edge; spheres form eventually along the plate edges. (c) Internal boundaries within the plates can lead to plate splitting, followed by cylinderization (or edge spheroidization).

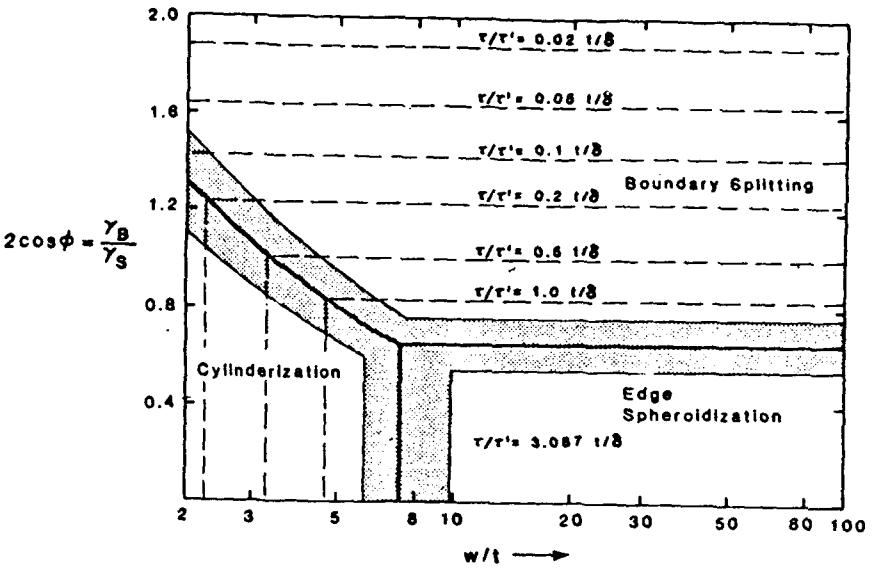

(a)

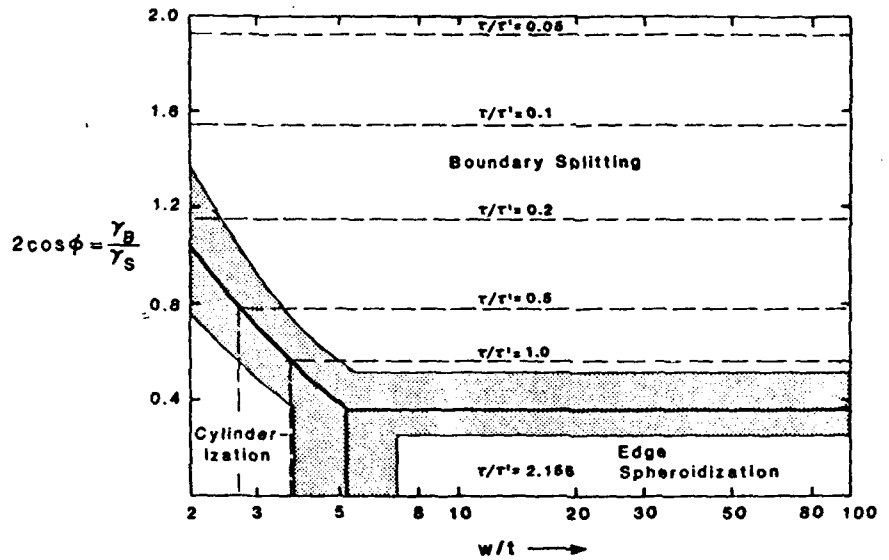

(b)

Fig. 2: Plate instability diagrams apropos for (a) surface diffusion control and (b) volume diffusion control of the process. The diagram is appropriate only for instabilities generated via intraplate diffusion. The areas of the diagram represent plate aspect ratio-dihedral angle combinations for which the specified instability mechanism dominates. Contours of the times required (in terms of a base, or normalized, time) to effect the instability are superimposed on the diagram. Shaded areas represent estimated uncertainties in the locations of the boundaries on the diagram.

subject so deftly handled in a clear and simple manner".

We were also invited to present a paper (A5) on this subject at the 12th Riso International Symposium. This paper expands our treatment to consider the instability problem when interplate diffusion can happen. This will be important when volume diffusion dominates the instability process and when the volume fraction of the plate phase is appreciable. Our extended treatment shows that edge spheroidization ought not to be observed when the above conditions hold. Instead, termination migration - in which mass is transferred from a lamellar termination to an adjacent plate, and which leads to recession of the termination - should take precedent over edge spheroidization. The results of this expanded treatment can be presented in the form of a "coarsening diagram" (Fig. 3). Such a diagram is somewhat similar to the ones of Fig. 2. However, in Fig. 3 the dominant coarsening mechanism (corresponding to the greatest rate of volume mass transport) is used to define the regions of the map. The diagrams, and the corresponding rates of mass transport, can be used to "semiquantitatively" follow plate breakdown. This is done in Fig. 4 where the internal surface area to volume ratio is plotted vs. (normalized) time at temperature, and schematics of the evolving plate geometry are also shown there for a plate with no internal boundaries and one having such boundaries.

B. Metal-Metallic Glass Composites

Publications (B1-B4) emanated from the doctoral work of Y. Leng. Of the papers, B3 and B4 are the most significant. We have been interested in the properties of metal-metal glass combinations for some time (see also Section D), and in fact had attempted to synthesize these by mechanical alloying metal powder and chopped metallic glass ribbons. However, the glass we used was so hard (and tough?) that it did not fragment during alloying. As a result we set our sights differently, and proceeded to investigate the mechanical characteristics of laminates of a metal (brass) and a nickel base metallic glass; this is a macroscopic prototype of the structure found on a fine level during MA.

Paper B1 dealt with the tensile properties (strength and ductility) of these laminates. Tensile strength was described well by a volume fraction rule. However, tensile elongatons of the glass in the composite exceeded that of monolithic glass. This was attributed to the (often) observed multiple shear banding of the glass in the composite (only a single shear band precedes tensile failure of monolithic glass). Paper B2 described some of our initial efforts at developing finite element techniques for analyzing composites of this type. In this paper the analysis was applied to the problem of calculating ineffective lengths in composites. The analysis was in accord with analytical expressions for the case of "well bonded" composites. However, the finite element technique was used to also consider the situations where fiber-matrix debonding and interfacial cracks

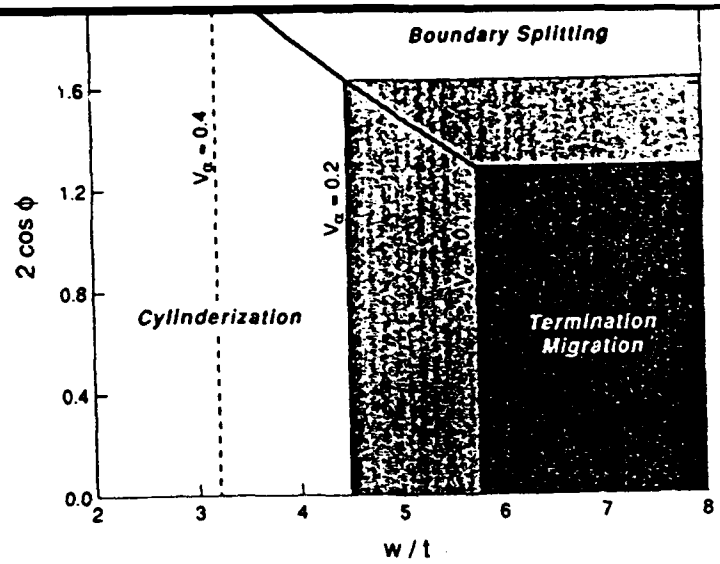

Fig. 3: A coarsening diagram for plate like structures. This diagram is appropriate when volume diffusion controls the instability processes and when interplate diffusion is significant. The respective areas of the diagram, which represent the dominant mass transfer rate, depend on the plate volume fraction. Termination migration supplants edge spheroidization as a dominant instability mode when the conditions stated above hold.

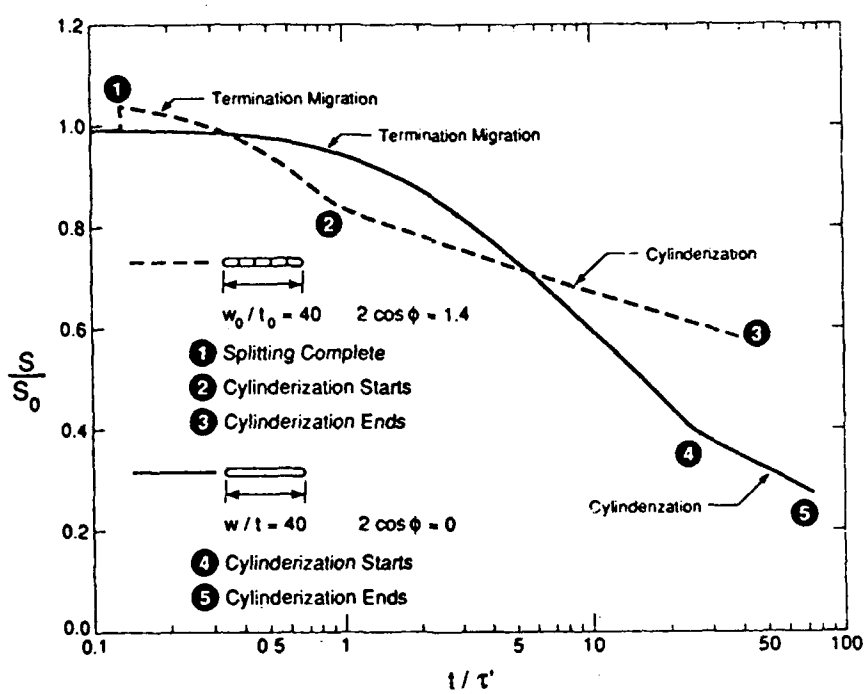

Fig. 4: Internal surface area change as a function of coarsening time for volume diffusion coarsening in a plate like structure having a plate volume fraction of 0.20. Two plates are considered. Both have initial aspect ratios of 40. One plate has (four) internal boundaries; the other has none. The latter coarsens by termination migration until the plate aspect ratio is reduced sufficiently for cylinderization to intervene (Point 4 in the figure). Cylinderization is completed at the time corresponding to Point 5. Plate splitting is completed at short times (Point 1) for the plate having internal boundaries. The plate fragments then coarsen by termination migration until their aspect ratios are low enough for cylinderization to take precedence (Point 2). Cylinderization of these is complete at the time corresponding to Point 3.

occur. Critical lengths were, understandably, greater for the fiber-matrix debonding case. We were also able to deduce effective stress concentrations for when interfacial cracks are present.

Paper B3 dealt with fracture toughness in these types of composites. Laminate crack growth resistance was considerably greater than that of monolithic glass. In addition, stable crack growth was observed in the composites whereas monolithic glass fails catastrophically. The increased toughness is both extrinsic and intrinsic in nature, with extrinsic toughening being most important. The crack in the glass extended beyond that in the brass, so that the latter provided an extrinsic crack closing force. (The tougher the brass, the greater this force.) Extrinsic toughening was well described by a particle toughening model developed by Shang and Ritchie, and which we extended to the laminate geometry. The intrinsic toughening results from the multiple shear banding of the glass. We were able to demonstrate that the magnitude of this toughening was of the same order as the inherent glass toughness and well below the crack growth resistance provided by the brass plates. The overall scheme is represented in Fig. 5, which shows the several contributions to toughness as they depend on crack length.

Paper B4 determined "distribution" functions for shear band initiation in the metallic glass. This was done by determining the frequency of shear banding as a function of stress level in bend tests (Figs. 6 and 7). We then used a finite element technique, which predicted the stress intensity associated with a shear band in a tensile test of a laminate, to determine the tendency for multiple shear band formation in laminates. Successful correlation with our observations and (different) ones of Embury and coworkers were made on the results of the analysis.

C. Deformation Processed Composite Materials

Paper C1 represented work accomplished during the 1985-88 grant period. It dealt with the conditions which lead to the transverse kinking observed during drawing of bcc transition metal fibers embedded in a fcc matrix.

In (C2), we tried to present a balanced overview of existing data relative to strengthening mechanisms in (DPCM). Our view has been that the incremental strengthening found in DPCM is "stored" in the structure as a result of the inherent strain incompatibility between the composite constituents. The alternative view - that strengthening arises from the two phase analog of a Hall-Petch mechanism - does not seem to us capable of explaining the high strengths of DPCM nor their tendency to soften on temperature exposure. Our viewpoint was challenged by proponents of the alternative mechanism which led to further, lively and (it is hoped) illuminating discussion (C3 and C4).

Our work in this area over the years resulted in two invited papers. One (C5) was a general overview of the processing,

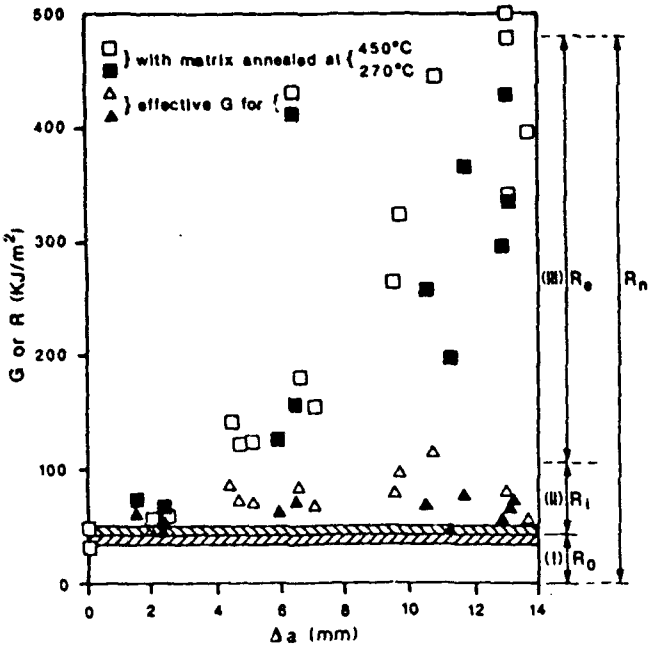

Fig. 5: Crack growth resistance curves for metal-metallic glass laminates as a function of crack length (in the glass). The curves are for a nickel base glass and a brass matrix in both a "soft" (annealed at 723 K) and hard (annealed at 543 K) condition. The hash base line represents the inherent toughness of the glass. It has the value stipulated as R_0. The triangles represent the toughening associated with multiple shear banding of the glass in the composite; this intrinsic toughening is denoted as R_i. The squares represent the extrinisic toughening (R_e) provided by the crack closing force of the brass. The softer (and tougher) matrix leads to increased values of R_e.

Fig. 6: Multiple shear bands, formed in bend tests, in metallic glass. Banding observed at two different stress levels ((a), a low stress, and (b), a higher one) is shown.

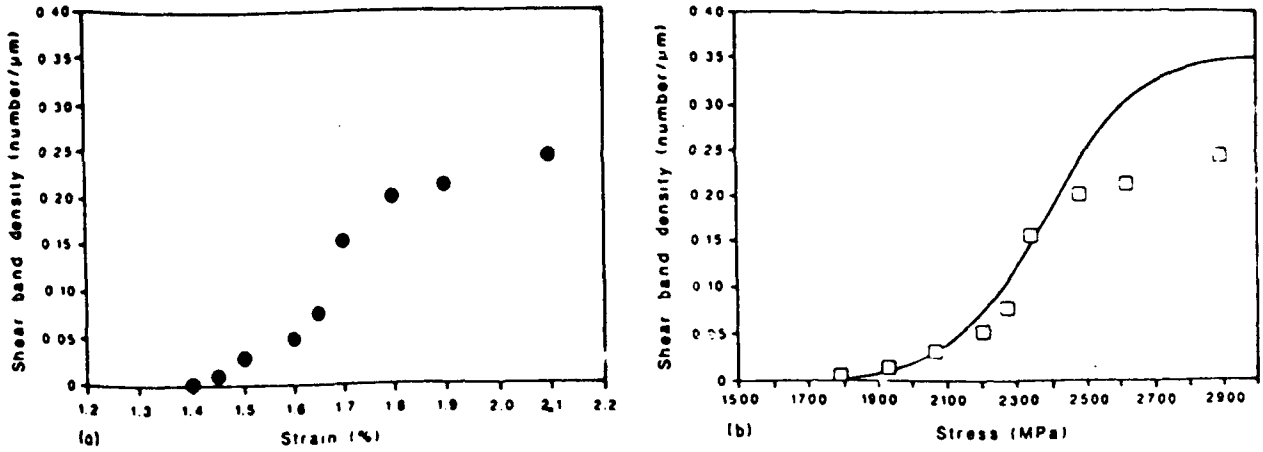

Fig. 7: (a) Shear band density (number per micrometer of length)in a nickel based metallic glass as a function of strain (b) Shear band density as a function of stress (converted from (a) by knowledge of the glass modulus). The solid line is a modifiedd Weibull function which repesents well the data in the low stress and strain region.

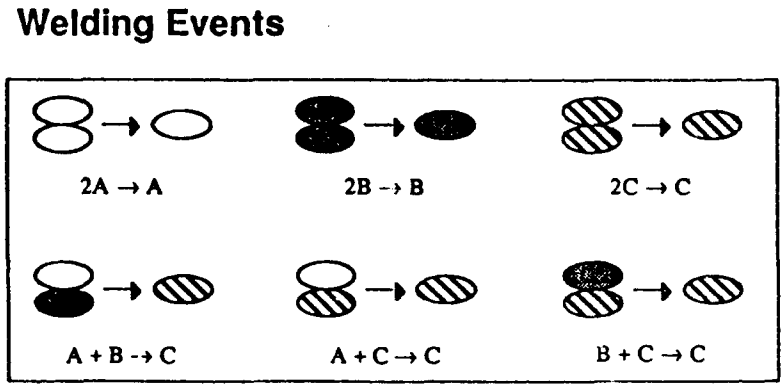

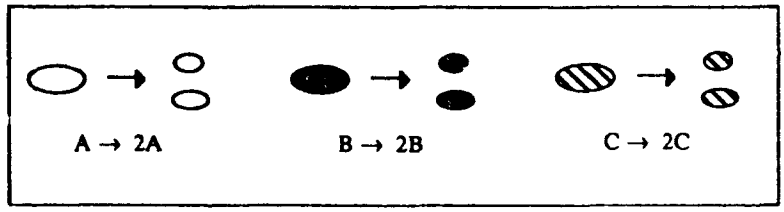

Fig. 8: Schematic of welding and fracture events taking place during MA. A and B represent elemental powder particles and C a composite or alloy particle. Welding events involving two common particles (e.g, A and A) remove one such particle from the population. When A and B coalesce, elemental powders are removed from the population and an alloy one is formed. When an elemental particle welds with an alloy one, the elemental particle is removed from the powder population. Fracture of any species results in addition of a particle of that species to the population.

structure and properties of DPCM, presented at the annual meeting of the American Society for Composites. The other (C6) dealt with strengthening mechanisms of DPCM and was drafted for the Treatise of Materials Science and Technology.

D. Mechanical Alloying

Various aspects of MA have been the focus of much of our work these past three years. Our efforts in the area have expanded significantly since they were first initiated in late 1986. We are basically interested in three facets of the MA process: process modeling, development of unique materials via MA and consolidation of mechanically alloyed powders. Some of our work is already in print and will be synopsized in this section. However some - not yet in print and in progress - will be described in more detail.

Our first efforts in modeling developed a simple, although fundamental, description of MA (D1). The model used elements of solid mechanics, materials science and engineering, fluid mechanics and heat transfer to define or estimate a number of variables for common MA devices. Mechanics was used to estimate the (Hertzian) radius of contact between impacting workpieces. This is legitimate as the presence of powder between colliding workpieces only mildly perturbs the collision. As a result we could also use Hertzian impact theory to define the collision duration. Impact velocities were estimated via simple modeling and experiments. The height of the porous powder "slug" caught between the colliding workpieces was estimated via simple fluid mechanics and geometry. Subsequent experiments confirmed the adequacy (within about a factor of two) of this estimate. Knowing the collision velocity, collision time and the volume of powder trapped between the workpieces allows powder strain rates and strain per collision to be estimated. In turn, and with the assumption of the plastic deformation work being adiabatically converted to heat, we found that the temperature rises during impact are modest (typically 10 to 100 K). We also showed that powders heated in this way cool down to the mill ambient temperature before being again impacted. Finally, we used the results of these modeling studies to estimate milling times needed to refine microstructure during MA. This was done on the basis of a certain accumulated process strain being required to yield the desired degree of refinement. The calculated milling times are of the correct order of magnitude for both an attritor and a Spex mill.

We extended this analysis in two other papers. In one (D2), we calculated the distribution of impact angles for several MA devices. This is important as the powder cold welding and fracture events taking place during MA depend on impact angle. Head-on impacts favor both types of events, whereas glancing impacts are less efficient in this regard. In another study (part of A4) we estimated the time required to effect "diffusion" during MA. Diffusion was defined as complete alloying of, say, two miscible elements. The model used the concept of strain per

collision to define the (changing) level of microstructural scale over which diffusion must take place during the processing. It also used the previously estimated temperature rise during impact, the impact time and time between collisions for the purpose of determining the extent of interdiffusion (per impact and per unit time). Alloying was considered complete when the cumulative interdiffusion distance equaled the instantaneous interphase "spacing". One question is what diffusion coefficient to use in the formulation. In particular, the very fine submicrostructure which characterizes ductile mechanically alloyed materials suggests enhanced diffusivities vis a vis typical lattice diffusion coefficients. Certainly the modest estimated temperature increases during impact seem insufficient to account for the extensive interdiffusion observed during MA.

We have also used quantitative metallography to estimate time constants for fracturing and welding during MA (D3). The idea is schematized in Fig. 8. Here the elemental (starting) powders are designated as A and B and an "alloy" particle as C. Three of the possible welding events (A-A, B-B and C-C) lead to removal of one particle of each species from the population. Two of the welding possibilities (C coalescing with A or with B) remove an elemental powder particle from the population, whereas when A and B coalesce an alloy powder is formed and elemental particles are concurrently removed from the population. Fracture events are easier to describe. When any kind of particle is fractured, an additional particle of the fractured species is formed.

A series of differential equations describe the time variation of the elemental and alloy powder population in terms of the coalescence and fracture probabilities *per collision* for the respective species. In our first attempt at analyzing process kinetics, we reduced these cumbersome expressions to more simple ones by assuming the probability of a fracture event per collision (α_f) was independent of particle species and that of a welding event (α_w) was likewise. On this basis, the total number of particles (N) in the population is given by

$$N/N_o = \exp[(\alpha_f - \alpha_w)t/\tau] \qquad (1)$$

where N_o is the original number of particles, t the milling time and τ the time between impact events for a given particle. We also derived an expression for the fraction of the population of particles that is, say, A:

$$[f_A/(1 - f_A)] = [f_{Ao}/(1 - f_{Ao})] \exp(-\alpha_w t/\tau) \qquad (2)$$

In Eq. (2), f_{Ao} is the original fraction of the population that is A. A corresponding equation holds for species B.

The analysis was applied to mechanically alloyed Cu-Nb alloys. Quantitative metallograpy was used to determine the fraction of elemental (unalloyed) Cu and Nb particles as a function of alloying time in an attritor, and for two different

charge ratios (CR= 10 and 50; CR= mass of grinding balls/mass of powder). The analysis reasonably describes the variation of Cu powder fractions. Higher charge ratios lead to reduced times to alloy; the time constants (τ/α_w) are ca. 1.8 and 7.8 hr., respectively. The time constant almost scales directly with CR as shown in Fig. 9, where the normalized time scale is the milling time multiplied by CR. Higher CRs lead to lesser coalescence times because the deformation per particle - and the resulting tendency to cold weld - is greater when there are fewer particles involved in a collision event.

The analysis also indicates an attritor is not a very efficient device for causing coalescence. For example, using our model of MA, the time between individual powder particle collisions in our attritor is on the order of 0.6 s (CR=10) and 3.0s (CR=50). On this basis, welding probabilities per collision are on the order of 10^{-4} to 10^{-5}.

Our simple analysis did not appear to mimic well the behavior of the Nb particles. In particular, they exhibited a reluctance to cold weld. At first we thought this indicated a flaw in the model. However, on the basis of refinements we have made in the model, we no longer believe this is so. Our refined analysis reduces the number of assumptions, although some remain. For example, we now assume the independence of welding and fracture events for A and B particles, but welding probabilities of C particles (to themselves and to A and B particles) and fracture events for C particles are weighted averages of the like occurences for elemental particles. The new expressions for the time variation of the elemental fractions of the particle population are

$$df_A/dt = Af_A(1-f_A) + Cf_Af_B \qquad (3a)$$

and

$$df_B/dt = A'f_B(1-f_B) + C'f_Af_B \qquad (3b)$$

where

$$A = -\alpha_{AA} + V_B(\alpha_A - \alpha_B)$$

$$C = (1- V_B)(\alpha_A - \alpha_B)$$

where V_B is the volume fraction of the aggregate that is elemental B. In Eqs. (3), α_{AA} is the probability per collision of an A particle welding to itself, and $\alpha_{A,B}$ are the corresponding fracture probabilities of A and B particles. The coefficients A' and C' are of form similar to A and C, except that the subscripts for species A and B are interchanged.

Equations (3) are nonlinear differential equations having no analytical solution, as far as we know (and as far as the three mathematicians we have consulted know). However, they can be integrated numerically, and series solutions can also be obtained

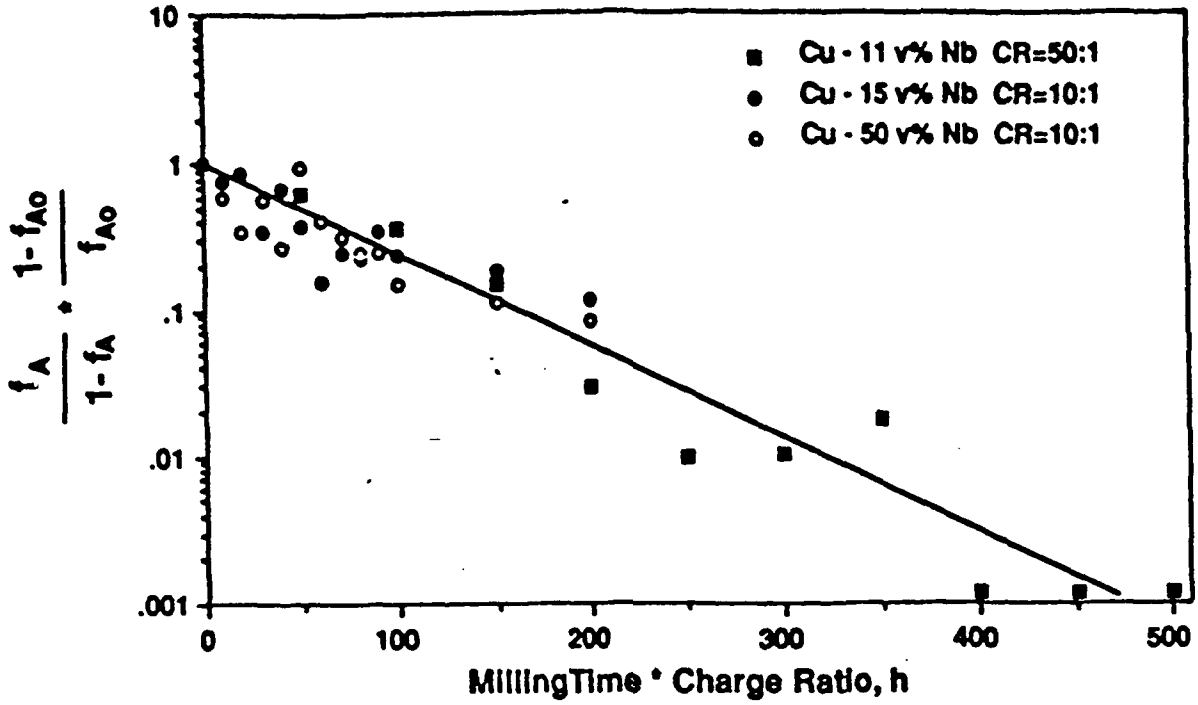

Fig. 9: Normalized particle fractions of Cu (cf. Eq. 2) vs. "normalized" milling time for mechanical alloying of Cu and Nb in an attritor. The normalized time is the product of the milling time and the charge ratio. A plot like this is useful for determining the time constant for welding of copper particles during MA, as described in the text.

which can be fitted to experimental results. This enables us to determine the respective welding and fracture probabilities for the various species. We are now in the process of using data we have obtained experimentally in this way, as elaborated on below.

We have mechanically alloyed Cu-Nb, Cu-Fe and Cu-Cr (containing 15 vol% of the bcc transition metal) in an attritor. The several bcc metals investigated have differing mechanical and surface characteristics. Chromium is the least malleable of these and also has a tenacious oxide surface. Niobium and Fe are ductile, but iron's surface film is less protective than that of Nb. Some results are shown in Figs. 10 and 11, where the distribution of the particle sizes of the several material combinations are shown as a function of milling time. These results are for a specific atmosphere (90% argon- 10% oxygen). Figure 10 shows a cumulative weight distribution of the several alloy systems studied. The figure shows that alloys containing Cr manifest a greater tendency to fracture or reluctance to weld than do the others (as reflected by the greater weight percentage of "small" particles in the Cu-Cr mixture). Figure 11 presents these same data (for an ambient milling temperature) in terms of a differential distribution which is another way of viewing these same phenomena. We are now in the process of developing the software required to extract the rate constants for fracture and coalescence, using our refined kinetic model. We believe (hope?) these can be tied directly to the fundamental process model we have developed. As ancillary data, we have also obtained, using x-ray line broadening studies, residual strain and "crystallite" size (these are on the order of nanometers) as a function of milling time for the respective materials. We do not yet know how these can be correlated to, say, fracture probabilities but there clearly must be some link between material substructure and fracture tendencies. The work described represents the continuing effort of Ms. Aikin whose Ph.D. requirements should be met sometime later this year or early next year. At that time we expect to be able to present a more comprehensive story. The problem is an intriguing one, and to our knowledge this is the only study being conducted along the tack we are pursuing.

We have also been actively investigating the amorphization and crystallization behavior of Ni-W alloys* and the consolidation behavior of these materials during hot isostatic pressing

*-Results described here represent the combined efforts of A. Aning and Z. Wang. Dr. Aning, a faculty member at Morgan State, visited us for a one year period during which time he was supported through a DARPA/NASA program. Aning initially intended to involve himself in modeling studies, but soon after his arrival he discovered the Ni amorphization reaction. Mr. Wang was to study the technological implications of mechanically alloyed Ni-W studies (and is doing so, see later discussion), but Aning and Wang combined efforts in order to fully clarify the factors underlying the amorphization reaction and the thermal stability of the amorphous phase.

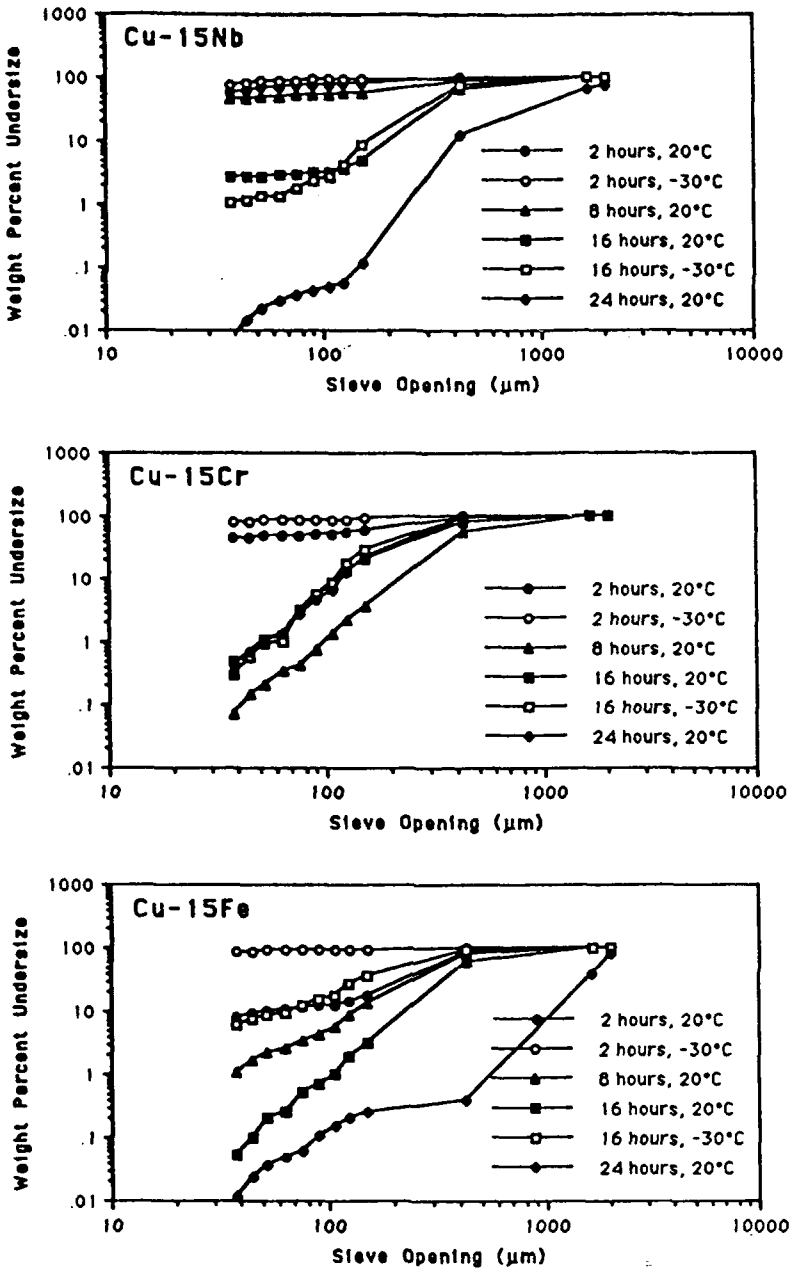

Fig. 10: Cumulative weight distributions for Cu-bcc transition metal combinations after milling in an attritor. Due to welding the fine initial particles become larger with increased milling time. The data indicate that alloys containing Cr exhibit a greater reluctance to weld than those containing Fe and Nb.

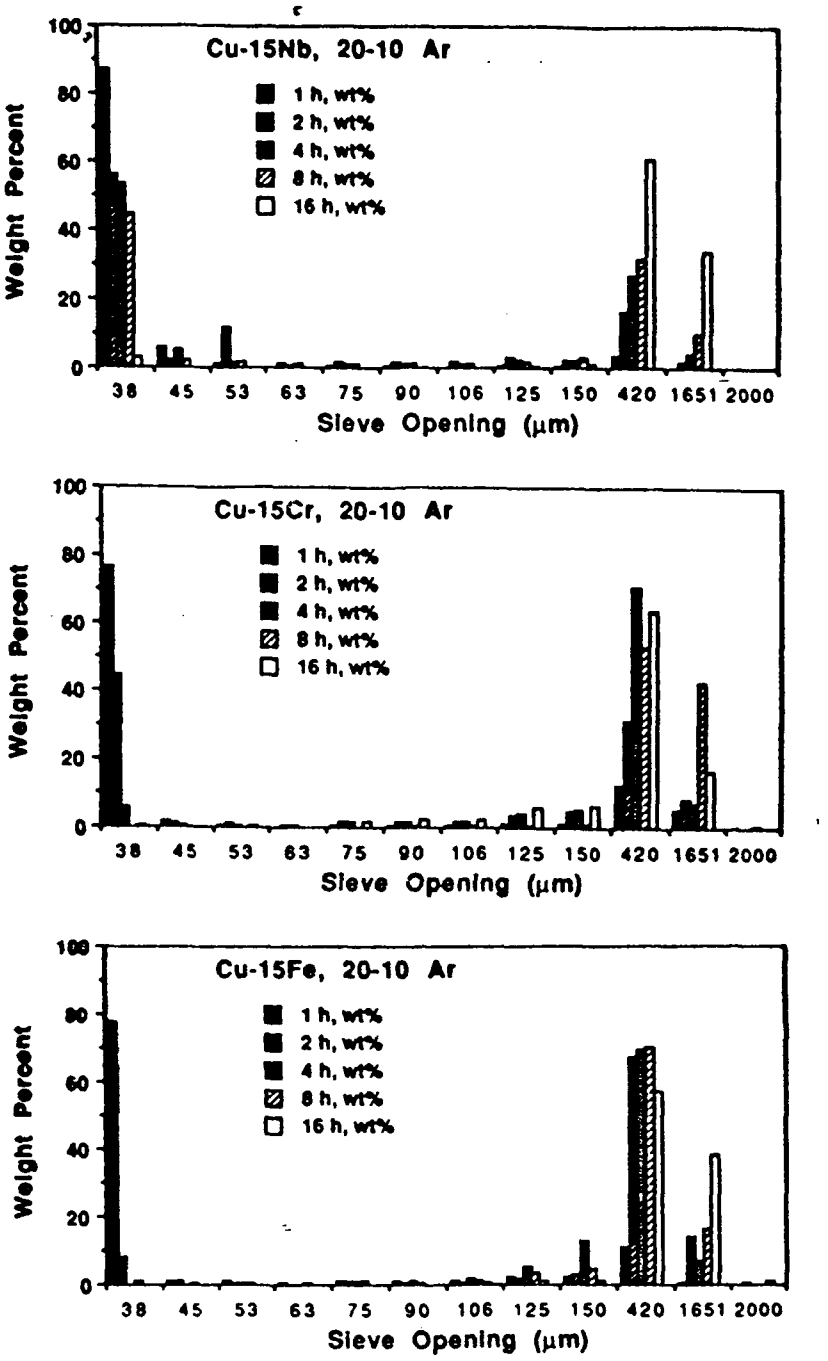

Fig. 11: The data of Fig. 11 represented as a differential distribution. The larger particles that form on increased milling time are a result of the welding taking place during MA. The analysis described in the text is currently being applied to data such as this to determine welding and fracturing probabilities.

(HIPping) (D4 and continuing studies). Amorphization is conveniently followed by x-ray diffraction (Fig. 12), but we have also confirmed amorphization by direct transmission electron microscopy. The gradual replacement of Ni crystalline peaks by amorphous ones, as a result of alloying, is indicated in Fig. 12. Prior to amorphization the crystalline Ni peak is displaced, indicating solution of W within this phase which is simultaneously evidenced by the diminished intensity of the W crystalline peaks (Ni does not dissolve in W to any significant extent). In addition the crystalline peaks of both the Ni rich and the W phase are broadened as a result of the fine substructure developed accompanying cold work during MA (crystallite sizes are in the range of 5 to 15 nm. after several hours of milling in a Spex mill).

The extent of solution of W in Ni can be followed so long as the Ni phase lattice parameter can be measured accurately. This allows us to determine the W content of this phase. We find that for overall W contents less than ca. 28 at.%, all of the W dissolves in crystalline Ni and amorphization does not take place. It is noteworthy that MA induces extended solubility; the equilibrium solubility of W in Ni at room temperature is only about 16 at.%. For W contents in excess of the critical 28 at.%, amorphization takes place. By measuring integrated intensities of the W phase and the Ni crystalline phase (taking into account the increase in scattering power caused by W solution in the latter) we were able to "semiquantitatively" deduce the respective phase volume fractions during the initial stages of milling. Some results are shown in Fig. 13. The volume fraction of the Ni crystalline phase initially increases as a result of W dissolution within it (solution precedes amorphization). At longer milling times, the amorphous phase increases at the expense of both crystalline phases. It is also interesting that this analysis indicates that some amorphization takes place before it is evident in the x-ray diffraction pattern (compare Figs. 12 and 13).

We have used differential scanning calorimetry to follow the crystallization behavior of the amorphous phase. As shown in Fig. 14, the crystallization temperature is fairly high (on the order of 1000 K) and increases with milling time indicating to us that the W content of the amorphous phase continues to increase with extended milling. The crystallization products vary, depending on the overall alloy composition. X-ray diffraction subsequent to crystallization reveals, depending upon these parameters, combinations of Ni, W and intermetallic compounds (Ni_4W and NiW).

We have also carried out consolidation studies (via HIPping) of these materials. This work (of Mr. Wang) is in progress, so a "full" story is not available at this time. However, we have not (at least not yet) been able to retain the amorphous phase and simultaneously attain full density. Attainment of full density requires higher HIPping temperatures than the crystallization one. Some results of our densification studies are shown in Fig. 15. Figure 15a is an optical micrograph of an almost fully

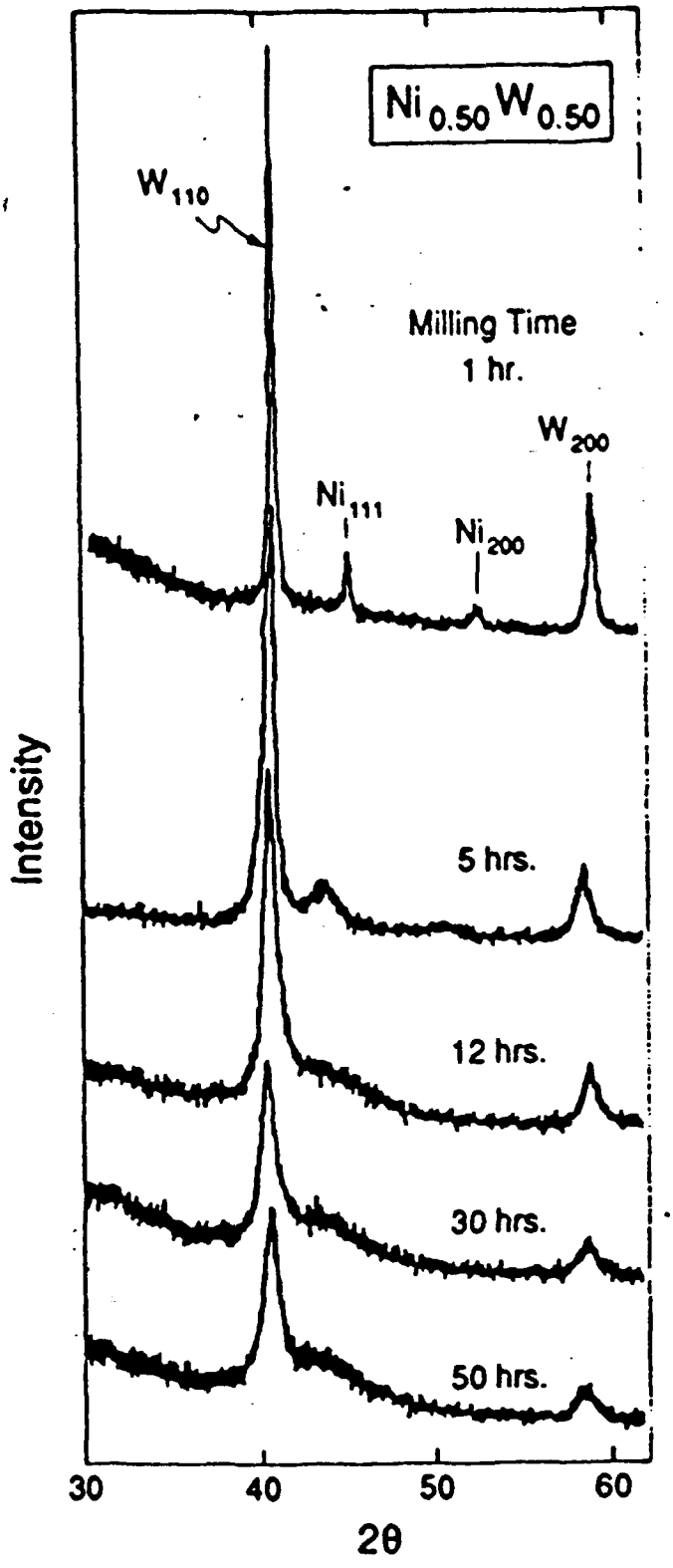

Fig. 12: X-ray diffraction patterns of an equiatomic Ni-W alloy after milling for different times in a Spex mill. With increased milling time, the Ni crystalline peaks become more diffuse. The Ni crystalline phase is essentially supplanted by the amorphous Ni phase for milling times of 12 hr. or more. The peak positions of the Ni crystalline phase are shifted for times less than this, indicating W solution in the Ni. Tungsten peak positions do not shift, but their intensities decrease during milling as a result of the solution of W in the Ni rich phases.

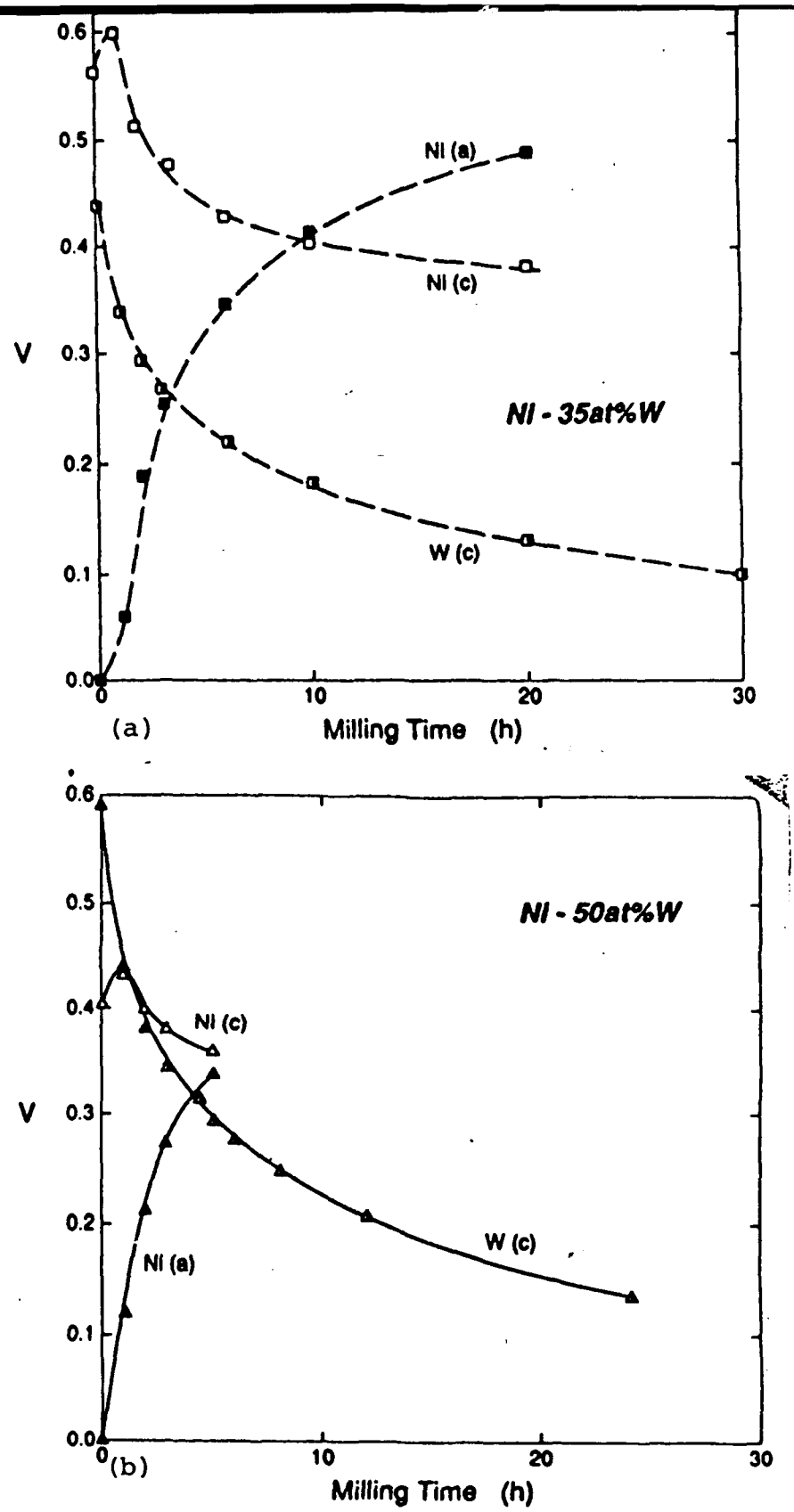

Fig. 13: Relative crystalline W, crystalline Ni and amorphous phase volume fractions as a function of milling time for (a) a Ni-35 at.%W alloy and (b) a Ni-50 at.%W alloy. Phase volume fractions are approximated through analysis of x-ray integrated intensities. The analysis is good only for relatively short milling times, when the crystalline peaks of Ni are still apparent. The fraction of the Ni crystalline phase increases initially as a result of W solution within it. It is apparent the amorphous phase forms fairly early on in the process.

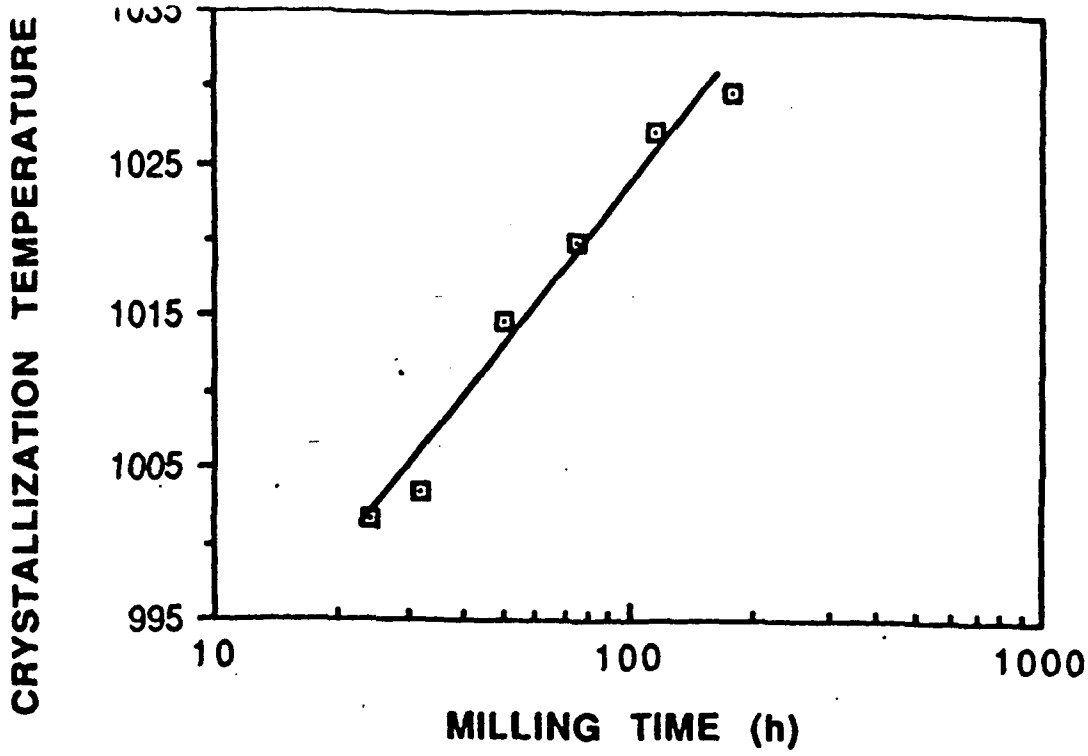

Fig. 14: Crystallization temperature vs. milling time for an amorphous Ni-50 at.% W alloy as a function of milling time. The increased crystallization temperature with further milling suggests a continuing solution of W in the amorphous Ni matrix.

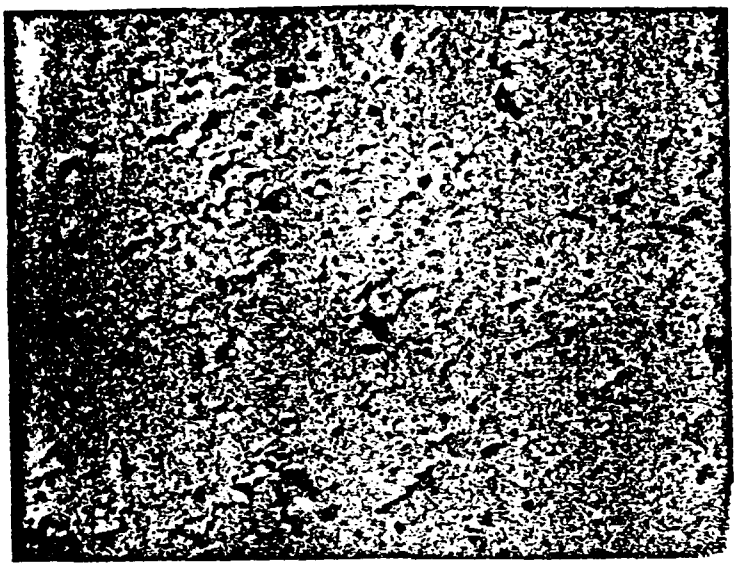

(a)

(b)

Fig. 15: (a) Optical micrograph of an almost fully dense Ni-40 at.% W alloy. The original powder was milled for 40 hrs. It was then consolidated by hot isostatic pressing (2 hrs at 973 K followed by 7 hrs. at 1223 K; pressure=25,000 psi). The fine structure of the consolidated product (on the order of tenths of micrometers) cannot be resolved at this magnification (500 X). (b) Scanning electron micrograph of an alloy HIPped under identical conditions as in (a). The composition of the alloy is the same except that 10 vol.% of Ni has been added to it. This nickel (the dark phase) allows for complete densification. The fine microstructural scale of the consolidated material can be barely discerned at this mangnification.

dense hot isostatically pressed Ni-40 at.% W alloy which had been milled 40 hrs. at room temperature. The amorphous phase is not retained during HIPPing. The phases formed during consolidation are NiW, Ni_4W and W; the fine scale of them cannot be resolved in this optical micrograph. As shown in Fig. 15b, full density can be attained under the same HIPping conditions pertinent to Fig. 15a if nickel is added in small amounts (10 vol.%) to the initial powder mix. The nickel is represented by the black areas in the scanning electron micrograph. The very fine scale of the other phases can be noted; they are barely resolvable at this magnification. We note that while the scale of the consolidated structure might be large in comparison to the initial mechanically alloyed structure, the overall scale of the consolidated structures is very fine. Indeed, in comparison to conventional heavy metal alloys which are made by liquid phase sintering and which have phase dimensions on the order of tens of micrometers, the scale of consolidated structures made from the mechanically alloyed materials is much less. This suggests the possibility of producing both stronger and tougher heavy metal alloys, and is an avenue we are now pursuing.

Consolidation studies have also been conducted on mechanically alloyed Cu-Nb alloys, the topic of Mr. Vance's recently completed M.S. thesis. This is an important area as the hardnesses of mechanically alloyed crystalline powders are impressive. In fact, conventional sintering of them is difficult to effect as the precursor cold pressing usually produces a friable green compact. Thus "brute force" techniques (e.g., extrusion, HIPping) are needed to consolidate such powder. Figure 16 provides reinforcement of these concepts. In this figure the room temperature yield strength (deduced from hardness measurements) is plotted as a function of one hour annealing temperature for "ordinary" copper, milled copper and a mechanically alloyed Cu-15 vol.% Nb alloy. As-milled and as-mechanically alloyed hardnesses are impressive (about three times those of ordinary copper). However, while the milled copper softens appreciably on heating, the mechanically alloyed material does not. This indicates that mechanisms of densification which devolve on dislocation activity (time independent yielding and power law creep) ought to be much different in mechanically alloyed materials than in conventional materials.

Mr. Vance studied the densification behavior during HIPping of four material systems: 1) unmilled copper, 2) milled copper, 3) a mixture of copper and 15 vol. % Nb and 4) mechanically alloyed Cu-15 vol.% Nb. Densification studies of the latter were most interesting, and will be discussed at most length here. Before doing this, though, we will synopsize the results of densification studies of the other materials.

Pure copper behaves rather much as expected during HIPping, but the analysis of densification was complicated since our starting powder (produced by a solidification technique) was quite porous (about 25 % by volume). This porosity was isolated (closed). That is, it was intraparticle from the outset of

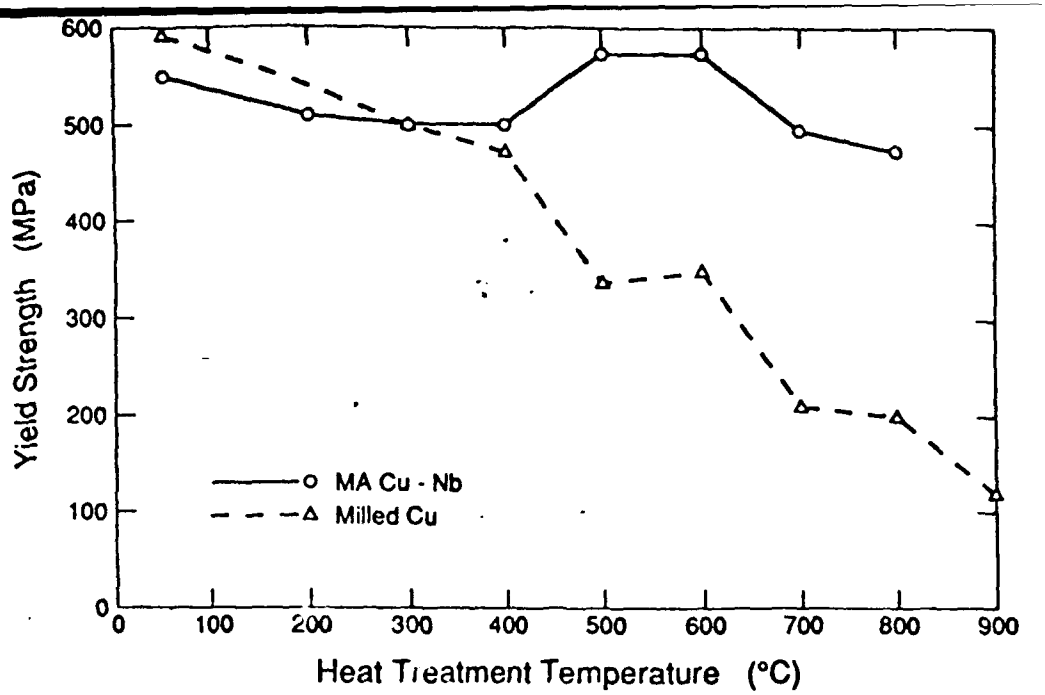

Fig. 16: Room temperature hardness equivalent yield strength after annealing for one hour at the specified heat treatment temperature for milled Cu and mechanically alloyed Cu-15 vol.% Nb. The milled elemental Cu softens appreciably on annealing. In contrast, the mechanically alloyed Cu-Nb does not. As milled or mechanically alloyed hardnesses are about three times those of unmilled Cu. (The increase in strength of the mechanically alloyed material on annealing in the temperature range 773-873K results from a precipitation effect.)

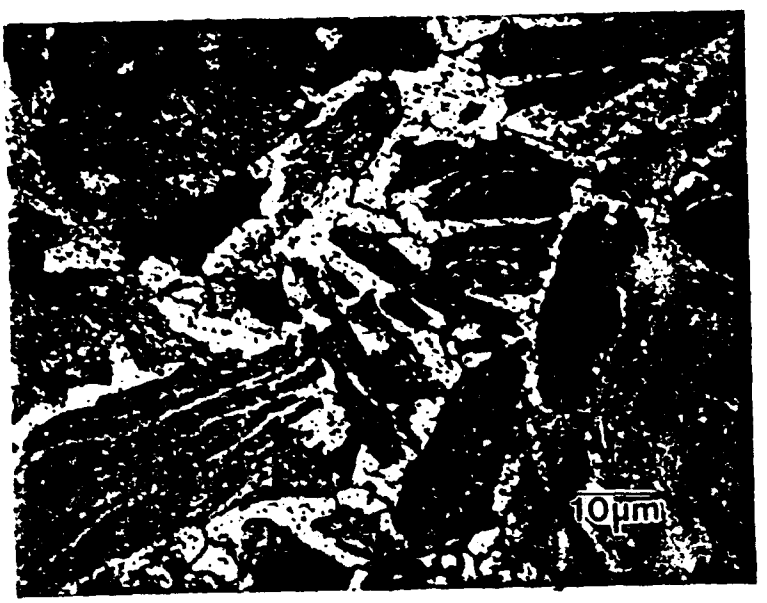

Fig. 17: Micrograph of a partially densified (80.8% of theoretical) mechanically alloyed Cu-Nb alloy. The powder was consolidated by hot isostatic pressing at 873 K for one hour and at a pressure of 27.6 MPa. Interparticle voids are being filled by Cu (the white phase), which creeps from within the "lamellar" structure of the mechancially alloyed powder. The grey microconstituent is a mixture of Cu and Nb; the two separate phases cannot be resolved at this magnification.

HIPping. Existing models of HIPping assume closed porosity is obtained only when the density reaches a fairly high (ca. 92% of theoretical) value. Thus existing models do not mimic well the densification behavior of our starting copper powder. On the other hand, the microstructural evolution during densification was "classical"; i.e. readily identifiable necks were formed between particles and the intraparticle porosity quickly became situated at grain boundaries. Moreover, full density could be readily attained at fairly high HIPping pressures (ca. 138 MPa) and temperatures (ca. 1200 K).

The morphological evolution during densification of (non mechanically alloyed) Cu-Nb mixtures was different. The last porosity to be eliminated was associated with Nb interfaces; either at Nb-Nb contacts or at interphase contacts. Full density could also be attained at the higher HIPping pressures and temperatures.

The densification behavior of milled Cu powder differed from that of unmilled Cu and unmilled Cu-Nb mixtures. First, as a result of milling, the particle size was greater and the size distribution broader. Milling also reduced the extent of intraparticle porosity to about 6 vol. %. This porosity took the form of "interlamellar" porosity; i.e., it was located between the lamellae of Cu (aggregates of such constitute the milled particles). Junctures, rather than well defined necks, formed during densification. This could be a result of the greater particle size, which reduces surface diffusion leading to "classically" shaped necks, and/or a change in densification mechanism. Finally we did not attain full density at the highest pressures (138 MPa) and temperatures (1273 K) investigated. Remnant porosity was interlamellar in nature, and it was hypothesized that entrapped gas prevented full densification.

Mechanically alloyed mixtures densified with an intriguing microstructural evolution. Copper was "squeezed" (probably by power law creep mechanisms) from interlamellar locations to the interparticle voids (Fig. 17). Almost theoretical density (ca. 98.5%) could be achieved at the highest HIPping pressures and temperatures used. The remnant porosity was interlamellar in nature, and residual from that (ca. 4%) existing within powder particles following MA. As shown in Fig. 18, densification behavior of the mechanically alloyed powders could be mimicked rather well using the concepts and computer programs apropos to HIPping as developed by Ashby. We altered the properties used in the analysis from that of pure Cu; primarily by changing the yield strength and temperature dependence of yield to reflect that of the mechanically alloyed material rather than that of "ordinary" Cu. The constitutive equation for power law creep of pure Cu was used in the analysis. Thus the agreement might be fortuitous, since it would be expected that the creep behavior of copper in the composite ought to be different from that of pure Cu (e.g., Fig. 16).

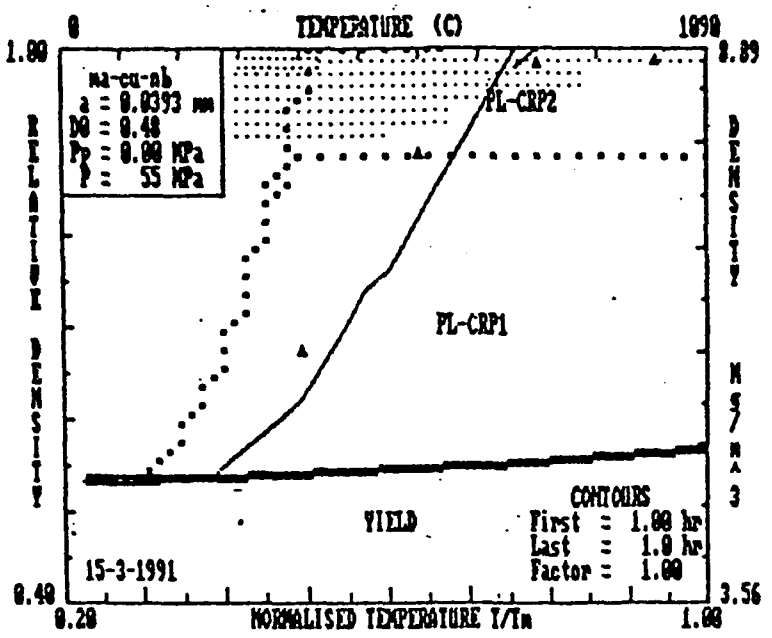

Fig. 18: Density vs. HIPping temperature (pressure=55MPa) for a mechanically alloyed Cu-15 vol. % powder aggregate. The triangles represent experimental data. These data are superimposed on a HIPping diagram, which was constructed on the basis of the properties of pure Cu, except for alterations representing the different yield strength and temperature dependence of yield for the alloyed material (cf. Fig. 16). The curve represents predicted densities, which agree fairly well with those experimentally measured. The regions of the diagram designate the dominant densification mechanism; in this case, by time independent yielding initially followed by power law creep.

III. SUMMARY

The work described here represents a broad approach to the problems of processing and properties of two phase solids, with particular emphasis on heavily deformed materials (as in DPCM which was our earlier focus and MA, our recent one). Details of the approach and accomplishments have been outlined in the preceding sections. It is clear that this area is a challenging one, encompassing many aspects of materials science and engineering. Kinetics, thermodynamics, microstructural stability, mechanical behavior and processing science all fall within the purview of a program like this one. We are currently using these same tools in our continuing study on various facets of MA, including the process itself and factors relating to consolidation of mechanically alloyed powders and their resulting properties.

APPENDIX A: ARO SPONSORED PUBLICATIONS JUNE 1, 1988-MAY 31, 1991

A. Microstructural Evolution and Stability

*A1. J. C. Malzahn Kampe, T. H. Courtney and Y. Leng, "Shape Instabilities of Plate Like Structures - I. Experimental Observations in Heavily Cold Worked In Situ Composites", Acta Metall., 37, 1735, (1989).

*A2. T. H. Courtney and J. C.Malzahn Kampe, "Shape Instabilities of Plate Like Structures - II. Analysis", Acta Metall., 37, 1747, (1989).

*A3. J. K. Lee and T. H. Courtney, "Two-Dimensional Finite Difference Analysis of Shape Instabilities in Plates", Metall. Trans. A, 20A, 1385. (1989).

**A4. T. H. Courtney, J. C. Malzahn Kampe, J. K. Lee and D. R. Maurice, "Modeling of Microstructural Evolution: Applications to Shape Stability and Mechanical Alloying", Diffusional Analysis and Applications, A. D. Romig, Jr. and M. A. Dayananda, Eds., TMS-AIME, Warrendale, Pa., 211, (1989).

**A5. T. H. Courtney, "Elevated Temperature Morphologcal Instabilities in Metal Matrix Composites", 12th Riso International Symposium on Metallurgy and Materials Science; Metal Matrix Composites, Roskilde, Denmark, Sept. 1991.

B. Metal-Metallic Glass Composites

B1. Y. Leng and T. H. Courtney, "Some Tensile Properties of Metal-Metallic Glass Laminates", J. Matls. Sc., 24, 2006, (1989).

B2. Y. Leng and T. H. Courtney, "Ineffective Lengths in Metal Matrix Composites", Matls. Sc. and Eng., A124, 141, (1990).

B3. Y. Leng and T. H. Courtney, "Fracture Behavior of Laminated Metal-Metallic Glass Composites", Metall. Trans. A., 21A, 2159, (1990).

B4. Y. Leng and T. H. Courtney, "Multiple Shear Band Formation in Metallic Glasses in Composites", J. Matls. Sc., 26, 588, (1991).

C. Deformation Processed Composite Materials

*C1. J. C. Malzahn Kampe and T. H. Courtney, "Transverse Kinking of BCC Fibers in Drawn FCC(Matrix)-BCC(Dispersoid) In Situ Composites", Scripta Metall., 23, 141, (1989).

C2. P. D. Funkenbusch and T. H. Courtney, "On the Role of Interphase Barrier and Substructural Strengthening in Deformation Processed Composite Materials", Scripta Metall., 23, 1719, (1989).

C3. P. D. Funkenbusch and T. H. Courtney, "Reply to Comments on 'On the Role of Interphase Barrier and Substructural Strengthening in Deformation Processed Composite Materials", Scripta Metall. et Mater., 24, 1175, (1990).

C4. P. D. Funkenbusch and T. H. Courtney, "Further Comments on Strengthening in Deformation Processed Composite Materials (DPCM)", Scripta Metall. et Mater., 24, 1183, (1990).

**C5. T. H. Courtney, "Processing, Structure and Properties of Heavily Deformed Two Phase Metallic Materials", Proc. 5th Technical Conference of the American Society for Composites, 491, Technomic Publishing, Lancaster, Pa., (1990).

**C6. T. H. Courtney, "Strengthening Behavior of In Situ Composites", Treatise Materials Sc. and Tech., R. K. Elliot and R. J. Arsenault, Eds., 33, 101, (1991).

D. Mechanical Alloying

D1. D. R. Maurice and T. H. Courtney, "The Physics of Mechanical Alloying: A First Report", Metall. Trans. A., 21A, 289, (1990).

**D2. T. H. Courtney and D. R. Maurice, "Some Fundamental Physics of the Mechanical Alloying Process", Solid State Powder Processing, A. H. Clauer and J. J. deBarbadillo, Eds., TMS-AIME, Warrendale, Pa., 3, (1990).

D3. B. J. M. Aikin, T. H. Courtney and D. R. Maurice, "Reaction Rates During Mechanical Alloying", accepted for publication in Matls. Sc. and Eng.

***D4. A. O. Aning, T. H. Courtney and Z. Wang, "Amorphization and Crystallization of Nickel in Mechanically Alloyed Ni-W Alloys", submitted for publication.

*- Indicates paper resulting from work conducted during immediately preceding ARO grant (1985-1988).

**- Indicates invited paper

***- Partial support from ARO and from DARPA/NASA

APPENDIX B: STUDENTS SUPPORTED AND DEGREES GRANTED JUNE 1, 1988-MAY, 31, 1991

B. J. M. Aikin (Ph.D. expected December, 1991)
Y. Leng (Ph.D., February, 1989)
D. R. Maurice (M.S., August, 1988)
R. R. Vance (M.S., June, 1991)
Z. Wang (M.S. expected August, 1991)